

# APPLICATIONS ON CRITICAL STATE SOIL MECHANICS USING A FINITE ELEMENT MODEL BASED ON EXPLICIT INTEGRATION AND ONE-POINT QUADRATURE

Alexandre Luis Braun, [allbraun@ig.com.br](mailto:allbraun@ig.com.br)

Armando Miguel Awruch, [amawruch@ufrgs.br](mailto:amawruch@ufrgs.br)

Programa de Pós-Graduação em Engenharia Civil (PPGEC), Universidade Federal do Rio Grande do Sul (UFRGS)  
Av. Osvaldo Aranha, nº 99, 3º andar, CEP: 90350-190, Porto Alegre/RS, Brasil

**Abstract.** A numerical model for investigations on Critical State Soil Mechanics (CSSM) is presented in this paper. CSSM may be considered as an extension of the classical theory of Plasticity into the field of Soil Mechanics, which permits to determine the soil behavior using elastoplastic constitutive models. In the present work, the modified Cam-Clay yield criterion is implemented into the framework of a pre-existing code for static analysis of geometrically nonlinear structures. The elastoplastic constitutive equation is integrated using an explicit algorithm where the strain increment is divided into a number of sub-steps defined automatically by the numerical scheme. In addition, the algorithm includes numerical procedures to enhance the model accuracy, such as nonlinear behavior for the elastic range and algorithms to determine the yield intersection point, to handle elastoplastic unloading and to restore uncorrected stresses to the yield surface. Eight-node hexahedral finite elements with one-point quadrature are employed in the spatial discretization of the geometrical domain. In order to avoid the excitation of spurious modes, an efficient hourglass control is utilized in conjunction with a corotational formulation, which also contributes to the treatment of geometrical and physical nonlinearities. Finally, numerical simulations are performed to demonstrate the applicability of the present formulation.

**Keywords:** Critical state soil mechanics (CSSM), Elastoplasticity, Explicit stress integration, Finite Element Method (FEM).

## 1. INTRODUCTION

The use of numerical models to simulate geotechnical problems has strongly increased in the last decades. This growth is mainly due to expressive advances obtained in constitutive modeling of soils and other granular materials and the great reliability achieved by present numerical methods, such as the Finite Element Method (FEM). Since the pioneering works of Coulomb (1776) and Rankine (1857), the theory of plasticity has been applied to describe analytically the mechanical behavior of soils, which is entirely justified based on experimental observations that suggest irreversible behavior for strains, yield phenomena and shear-induced dilatancy. In this sense, computational efforts to analyze such problems are usually high, owing to nonlinear characteristics referring to the material and kinematical descriptions of the problem. Therefore, robust low-order finite element formulations using the one-point quadrature technique are welcome.

One of the most popular constitutive formulations based on critical state soil mechanics (CSSM) is the Cam-Clay model. The original Cam-Clay formulation was presented by Roscoe and Schofield (1963) and Schofield and Wroth (1968) using an elastic-plastic constitutive framework. Later, Roscoe and Burland (1968) proposed the Modified Cam-Clay model, where some drawbacks of the original formulation were eliminated. The original Cam-Clay yield surface presents a discontinuity for isotropic compression stress states, which leads to numerical difficulties to determine strain increments when an associated flow rule is employed.

In a finite element analysis where nonlinear materials are considered, stress updates are obtained from numerical integration of the constitutive equation, which is performed using implicit or explicit algorithms. The main difference between implicit and explicit integration schemes lies on how variables are evaluated: at known stress states for explicit integration methods or at unknown stress states for implicit ones. From previous investigations (see, for instance, Gens and Potts, 1988; Potts and Ganendra, 1994; Sloan et al., 2001; Zhao et al., 2005), one verifies that explicit algorithms are more indicated to reproduce complex stress-strain relations, such as those observed for critical state models.

In this work, the numerical model presented by Duarte Filho and Awruch (2004) is extended to cover problems with elastic-plastic constitutive models, particularly the Modified Cam-Clay model. An explicit integration scheme, similar to that presented by Sloan et al. (2001), is implemented into the former code in order to update stress states at the center of the finite elements. Classical problems, including a three-dimensional example, are simulated to demonstrate the accuracy of the present formulation for geotechnical applications.

## 2. ANALYTICAL MODEL

Considering a classical Lagrangean kinematical description in the Cartesian coordinate system and in the absence of temperature changes and inertial forces, the conservation equations for an infinitesimal volume  $d\Omega$  are reduced to the following expressions:

$$\int_{\Omega_0} \rho(\mathbf{X}, t_0) d\Omega = \int_{\Omega} \rho(\mathbf{x}, t) d\Omega \quad (1)$$

$$\nabla^T \boldsymbol{\sigma} + \mathbf{b} = 0 \quad (2)$$

where  $\mathbf{X}$  e  $\mathbf{x}$  are vectors containing components of material ( $X_i$ ) and spatial ( $x_i$ ) coordinates in a Cartesian coordinate system, respectively,  $t$  represents time,  $\rho$  is the specific mass,  $\nabla$  is the differential operator,  $\mathbf{b}$  is the body force vector and  $\boldsymbol{\sigma}$  is the effective stress tensor. A measure for the stress tensor must be chosen such that the stress-strain relation maintains its objectivity. In this work, the Cauchy stress tensor and the small strain tensor are utilized, which should be defined in a corotational reference system.

In this work, a nonlinear hypoelastic constitutive equation is considered to relate strain and stress measures in the elastic regime as follows:

$$\boldsymbol{\sigma} = \mathbf{D}^e \boldsymbol{\varepsilon} \quad (3)$$

with:

$$\mathbf{D}^e = \begin{bmatrix} K + \frac{4}{3}G & K - \frac{2}{3}G & K - \frac{2}{3}G & 0 & 0 & 0 \\ & K + \frac{4}{3}G & K - \frac{2}{3}G & 0 & 0 & 0 \\ & & K + \frac{4}{3}G & 0 & 0 & 0 \\ & & & G & 0 & 0 \\ & & & & G & 0 \\ & & & & & G \end{bmatrix} \quad (4)$$

where  $K$  and  $G$  are the bulk and shear moduli, respectively. The bulk modulus associates spherical pressure increments with volumetric strain increments while the shear modulus associates deviatoric stress and strain increments. For critical state models, the tangential form of these moduli are usually assumed to be dependent on the effective mean normal stress  $p$ , which are usually expressed as:

$$K = \frac{\partial p}{\partial \varepsilon_v^e} = \frac{1+e_0}{k} p = \frac{v_s p}{k} \quad (5)$$

$$G = \frac{1}{2} \frac{\partial q}{\partial \varepsilon_d^e} = \frac{3(1-2\nu)}{2(1+\nu)} K \quad (6)$$

where  $\varepsilon_v^e$  and  $\varepsilon_d^e$  are the volumetric and deviatoric parts of the elastic strain tensor  $\boldsymbol{\varepsilon}^e$ ,  $q$  is the deviatoric stress,  $e_0$  is the initial voids ratio,  $v_s$  is the specific volume,  $\nu$  is the Poisson's ratio and  $k$  is the slope of the unloading-reloading lines (URL) on a  $\ln p$ - $\nu$  plane (see Schofield and Wroth, 1968 for additional information). It is worth to notice that the stress dependence on  $K$  and  $G$  leads to a nonlinear elastic constitutive matrix  $\mathbf{D}^e$ . The secant forms of Eqs. (5) and (6) are obtained by integrating Eq. (5), which yields:

$$\bar{K} = \frac{p_0}{\Delta \varepsilon_v^e} \left[ \exp\left(\frac{v_s \Delta \varepsilon_v^e}{k}\right) - 1 \right] \quad (7)$$

and, consequently:

$$\bar{G} = \frac{3(1-2\nu)}{2(1+\nu)} \bar{K} \quad (8)$$

where  $p_0$  is the effective normal stress at the beginning of the strain increment  $\Delta \varepsilon_v^e$ .

The yield function for the Modified Cam-Clay model may be written as:

$$f = q^2 - M^2(pp_c - p^2) \quad (9)$$

where  $M$  is the slope of the critical state line and  $p_c$  is the preconsolidation pressure, which is related to the maximum effective pressure experienced by the soil mass. Hence, if a stress state leads to  $f < 0$ , it is assumed to be elastic and if a stress state leads to  $f \geq 0$ , it is assumed to be plastic.

The incremental stress-strain equation in the elastoplastic range is given as follows:

$$d\boldsymbol{\sigma} = \mathbf{D}^{ep} d\boldsymbol{\varepsilon} \quad (10)$$

with:

$$\mathbf{D}^{ep} = \mathbf{D}^e - \frac{\mathbf{D}^e \mathbf{a}_g \mathbf{a}_f^T \mathbf{D}^e}{A + \mathbf{a}_f^T \mathbf{D}^e \mathbf{a}_g} d\boldsymbol{\varepsilon} \quad (11)$$

where  $A$  is a hardening parameter and  $\mathbf{a}_g$  and  $\mathbf{a}_f$  are flow vectors based on the yield and plastic potential functions, respectively, which may be expressed as:

$$A = - \frac{\partial f}{\partial p_c} \frac{\partial p_c}{\partial \varepsilon_v^p} \frac{\partial g}{\partial p} \quad (12)$$

$$\mathbf{a}_f = \frac{\partial f}{\partial \boldsymbol{\sigma}} \quad ; \quad \mathbf{a}_g = \frac{\partial g}{\partial \boldsymbol{\sigma}} \quad (13)$$

### 3. NUMERICAL MODEL

Applying the Bubnov-Galerkin weighted residual method in conjunction with the Green-Gauss theorem over the momentum equation (Eq. 2), the following expression is obtained:

$$\int_{\Omega_E} (\nabla \delta \mathbf{u})^T \boldsymbol{\sigma} d\Omega_E = \int_{\Omega_E} \delta \mathbf{u}^T \mathbf{b} d\Omega_E + \int_{\Gamma_E} \delta \mathbf{u}^T \mathbf{t} d\Gamma_E \quad (14)$$

where  $\mathbf{t}$  is the traction vector,  $\Omega_E$  is the volume referred to element  $E$  and  $\Gamma_E$  represents its boundary surfaces, both considered in the FEM context.

Spatial coordinates and displacements are approximated at element level using the eight-node hexahedral finite element formulation, which may be expressed as:

$$\mathbf{x} = \mathbf{N} \mathbf{x}_E \quad ; \quad \delta \mathbf{u} = \mathbf{N} \delta \mathbf{u}_E \quad ; \quad \mathbf{u} = \mathbf{N} \mathbf{u}_E \quad (15)$$

where  $\mathbf{x}$ ,  $\delta \mathbf{u}$  and  $\mathbf{u}$  are the coordinate, displacement variation and displacement vectors evaluated within the element domain and  $\mathbf{x}_E$ ,  $\delta \mathbf{u}_E$  and  $\mathbf{u}_E$  are their respective nodal values. The column matrix  $\mathbf{N}$  contains the shape functions of the eight-node hexahedral element.

The final matrix format of Eq. (14) in the global system, considering the incremental approach, is given as follows:

$$\mathbf{K}_{n+1,i-1}^{\tan}(\mathbf{u}, \boldsymbol{\sigma}) \Delta \mathbf{u}_{n+1,i} = \mathbf{f}_{n+1}^{\text{ext}} - \mathbf{f}_{n+1,i-1}^{\text{int}}(\mathbf{u}, \boldsymbol{\sigma}) \quad (16)$$

where subscripts  $n + 1$  denote current position in the time marching with  $i$  and  $i - 1$  indicating current and previous iterative steps in the Newton-Raphson method. The vector of external forces  $\mathbf{f}^{\text{ext}}$  represents the right-hand side terms of Eq. (14), while  $\mathbf{K}^{\tan}$  and  $\mathbf{f}^{\text{int}}$  are referred to the tangent stiffness matrix and the internal force vector, respectively. The tangent stiffness matrix and the internal force vector are evaluated in the corotational coordinate system using the following expressions:

$$\hat{\mathbf{K}}_{n,i}^{\tan} = \int_{\Omega_E} \hat{\mathbf{B}}^T (\mathbf{D} + \mathbf{T}) \hat{\mathbf{B}} d\hat{\Omega}_E \quad (17)$$

$$\hat{\mathbf{f}}_{n,i} = \int_{\hat{\Omega}_E} \hat{\mathbf{B}}^T \hat{\boldsymbol{\sigma}}_i d\hat{\Omega}_E \quad (18)$$

where  $\hat{\Omega}_E$  is referred to the current element configuration in the corotational system,  $\mathbf{D}$  and  $\mathbf{T}$  are fourth order tensors related to the elastic constitutive equation and Truesdell rate terms, respectively, and  $\hat{\boldsymbol{\sigma}}_i$  is the corotational Cauchy stress tensor evaluated at iterative step  $i$  (see Braun and Awruch, 2008; Duarte Filho and Awruch, 2004 for further details). It is important to notice that  $\mathbf{T}$  vanishes for geometrically linear problems as well as  $\mathbf{D}$  becomes  $\mathbf{D}^e$  for elastic materials and  $\mathbf{D}^{ep}$  for elastoplastic materials. In order to solve the equilibrium equation, the tangent stiffness matrix and the internal force vector are brought back to the global coordinate system using objective transformations.

Element formulations based on reduced integration must be stabilized using hourglass control techniques in order to avoid numerical instabilities. In this work, volumetric locking is remedied using reduced selective integration, where the gradient matrix  $\mathbf{B}$  is decomposed into deviatoric and volumetric terms of the strain tensor  $\boldsymbol{\varepsilon}$ , with the last terms evaluated at the center of the element. In addition, deviatoric terms must be expanded using Taylor series at the center of the element up to bilinear terms. The same procedure is carried out over the stress tensor  $\boldsymbol{\sigma}$ . On the other hand, shear locking is removed by describing shear components of the strain tensor  $\boldsymbol{\varepsilon}$  in an orthogonal corotational coordinate system. Moreover, all shear components must be linearly interpolated in a single direction of the reference system. In order to evaluate the internal force vector accurately when distorted elements are considered, the gradient matrix obtained with reduced integration is replaced by uniform gradient submatrices defined by Flanagan and Belytschko (1981). Further details about the reduced integration scheme and the corotational reference system adopted in this paper may be found in Braun and Awruch (2008).

In elastoplastic analysis, strain increments  $\Delta\boldsymbol{\varepsilon}$  are imposed at element level based on the incremental solution obtained from the equilibrium equation. On the other hand, stress increments are dependent on the material behavior. Therefore, a trial elastic stress increment is usually considered as an initial estimative for the new stress state. If this new stress state does not lead to plastic yielding, the corresponding stress increment is taken as true. However, if plastic yielding is observed, the following system of ordinary differential equations must be solved:

$$\frac{d\boldsymbol{\sigma}}{dT} = \mathbf{D}^{ep} \Delta\boldsymbol{\varepsilon} \quad (19)$$

$$\frac{d\kappa}{dT} = \Delta\lambda B \quad (20)$$

with:

$$T = \frac{t - t_0}{\Delta t} \quad (21)$$

$$\Delta\lambda = \frac{\mathbf{a}_f^T \mathbf{D}^e}{A + \mathbf{a}_f^T \mathbf{D}^e \mathbf{a}_g} \Delta\boldsymbol{\varepsilon} \quad (22)$$

$$B = -\frac{A}{\partial f / \partial \kappa} = \frac{v_s p_c}{\lambda_{NCL} - k} \frac{\partial g}{\partial p} \quad (23)$$

where  $T$  is the artificial time, which is defined in the range  $0 \leq T \leq 1$ ,  $t_0$  is the time at the starting point of the load increment ( $\Delta t$ ),  $t$  is the time in a position within the load increment ( $\Delta t$ ),  $B$  is a hardening parameter,  $d\kappa$  is the hardening parameter increment, which is assumed to be the preconsolidation pressure increment  $dp_c$ , and  $\lambda_{NCL}$  is the slope of the normal compression lines (NCL) on a  $\ln p$ - $v$  plane (see Schofield and Wroth, 1968 for additional information).

Once the elastic fraction of the stress increment  $\Delta\boldsymbol{\varepsilon}$  is obtained, the plastic fraction of the strain increment  $\Delta\boldsymbol{\varepsilon}'$  is determined using:

$$\Delta\boldsymbol{\varepsilon}' = (1 - \alpha)\Delta\boldsymbol{\varepsilon} \quad (24)$$

and the stress state at the onset of the plastic yielding  $\boldsymbol{\sigma}_{yld}$  is calculated from:

$$f(\boldsymbol{\sigma}_0 + \alpha \bar{\mathbf{D}}^e \Delta\boldsymbol{\varepsilon}, \kappa_0) = 0 \quad (25)$$

where  $\alpha$  is a scalar to be determined considering the yielding condition expressed by Eq. (25).

In order to define initial conditions for the system of equations described by Eqs. (19) and (20), the stress state  $\sigma_0$  is updated to the stress state at the onset of the plastic yielding  $\sigma_{yld}$  and the hardening parameter  $\kappa_0$  is considered at the start of the strain increment  $\Delta\epsilon'$  where  $T = 0$  and  $t = t_0$ . By using the explicit Euler method, a substepping technique, as proposed by Sloan et al. (2001), is applied over the strain increment  $\Delta\epsilon'$  to find the stress state and the hardening parameter at the end of  $\Delta\epsilon'$ , where  $T = 1$ . Subincrements of  $\Delta\epsilon'$  are defined according to the artificial time increment  $\Delta T$ , which is calculated taking into account a local error measure obtained from the difference between a second order accurate modified Euler solution and a first order accurate Euler solution. Consequently, the size of the subincrements is automatically modified along the integration process. For a complete description of the numerical algorithm utilized in this work, readers are addressed to Sloan et al. (2001).

#### 4. NUMERICAL APPLICATIONS

##### 4.1. Bi-dimensional analysis of a rigid strip footing

A bi-dimensional analysis of a rigid strip footing resting on a soil layer is carried out in this section. Footing tests have been extensively used to validate numerical algorithms based on elastoplastic formulations applied to soil mechanics. This problem may be considered as a very difficult task for most of the numerical schemes due to strong rotations verified in the principal stresses and the singularity observed at the edge of the footing.

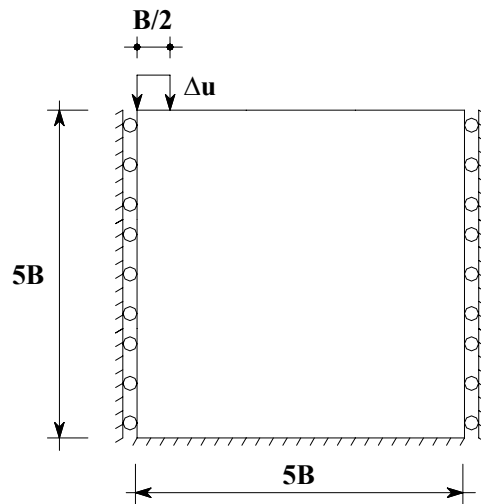


Figure 1. Geometry and boundary conditions utilized in the bi-dimensional rigid footing analysis.

All simulations are performed using the Modified Cam-Clay model and results are compared with numerical predictions obtained by Sheng et al. (2000). Comparisons are also carried out with respect to the geometrically linear and nonlinear approaches adopted in this problem. Geometry and boundary conditions utilized in the present study are shown in Fig. 1 and material parameters adopted in the Cam-Clay characterization of the soil mass are listed in Table 1. The computational domain is divided into 2703 eight-node hexahedral elements and plane strain conditions are imposed by restricting displacements in the orthogonal direction (axis  $z$ ). In order to simulate the action of the rigid foundation on the soil mass, uniform vertical displacements are applied along the footing-soil interface. It is important to notice that critical state models cannot mobilize any strength if the effective normal stress  $p$  is zero or tensile. Therefore, a compressive initial stress state must be established over the soil, which is accomplished in this example by considering a hydrostatic stress state generated from the soil specific weight. Moreover, the soil is assumed to be overconsolidated to 50 KPa at the ground surface, which implies that, at the ground surface, the preconsolidation pressure is 50 KPa.

Table 1. Physical parameters adopted in the rigid footing analysis.

Slope of CSL – $M$	0.898
Slope of NCL – $\lambda$	0.250
Slope of URL – $k$	0.050
Poisson's ratio – $\nu$	0.300
Specific weight – $\gamma$ [KN/m <sup>3</sup> ]	6
Initial void ratio – $e_0$	1.600

The load-displacement curves obtained in this work are presented in Fig. 2, where a prediction computed by Sheng et al. (2000) is also shown. As can be observed, a good agreement is verified when the geometrically linear model is considered. On the other hand, results obtained using the geometrically nonlinear approach lead to an overestimation of loads owing to an increase of stiffness, which is usually observed in this case. Displacements and footing loads are measured at the intermediate point underneath the footing, which correspond to the top left node of the computational domain.

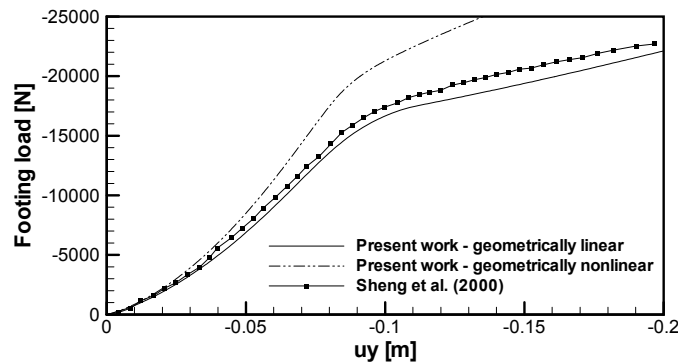


Figure 2. Load-displacement curves obtained in the rigid foot analysis.

Stress paths computed at the intermediate point underneath the footing are found in Fig. 3, where a good correlation can be observed when both the linear and nonlinear responses are compared to results presented by Sheng et al. (2000). As can be noticed, predictions obtained with geometrical linear and nonlinear models lead to very similar stress paths in the elastic range. However, some major differences can be observed after yielding.

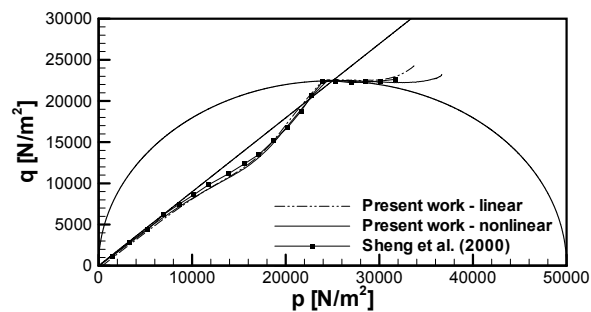


Figure 3. Stress paths obtained at the left edge underneath the footing.

#### 4.2. Bi-dimensional analysis of a flexible strip footing

The numerical simulation of the settlement induced by a bi-dimensional flexible strip footing is performed in this application. The present problem was proposed by Borja and Tamagnini (1998) to verify their critical state formulation, which is based on a Cam-Clay model. Comparisons of results obtained with the geometrically linear and nonlinear approaches utilized in this work are carried out over a flexible strip footing model represented by uniform vertical loads applied along the footing-soil interface.

Geometrical characteristics referring to the problem studied here are found in Fig. 4, where boundary conditions are also shown. The computational domain is divided into 540 eight-node hexahedral elements and all simulations are carried out considering an initial hydrostatic stress state  $p$  generated from the soil specific weight and plane strain conditions. Physical properties of the soil are presented in Table 2.

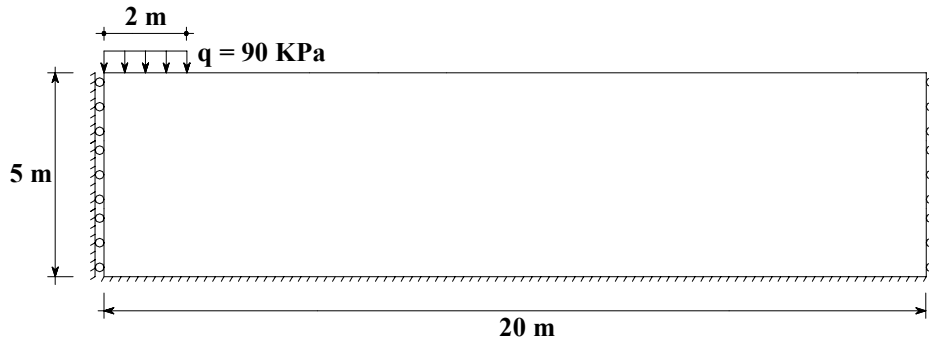


Figure 4. Geometry and boundary conditions utilized in the flexible footing analysis.

Table 2. Physical parameters adopted in the flexible footing analysis.

Slope of CSL – $M$	1.050
Slope of NCL – $\lambda$	0.130
Slope of URL – $k$	0.018
Initial void ratio – $e_0$	1.600
Poisson's ratio – $\nu$	0.250
Specific weight – $\gamma$ [KN/m <sup>3</sup> ]	10.000

Load-displacement curves computed in the present work are shown in Fig. 5 considering the different overconsolidation ratios ( $OCR = p_{c0}/p_0$ ) simulated here, where results obtained from Borja and Tamagnini (1998) are also presented. All predictions are measured at a point corresponding to the point of contact between the soil layer and the intermediate point underneath the footing, which correspond to the top left node of the computational domain. The best agreements between the reference work and simulations carried out here are referred to  $OCR = 2.50$  and  $OCR = 2.25$ , although the elastic behavior in these cases are distinct to that predicted by Borja and Tamagnini (1998), which is caused by different characteristics observed in the constitutive models compared in this example. As expected, the prediction obtained with the geometrically nonlinear model resulted in smaller vertical displacements when compared to that obtained with the linear model.

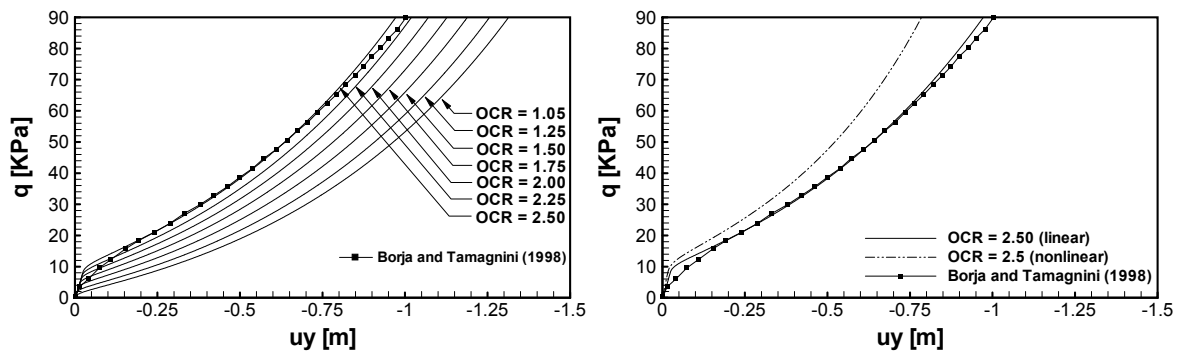


Figure 5. Load-displacements curves obtained in the flexible footing analysis.

Final mesh configurations and stress components obtained using geometrically linear and nonlinear models are compared in Fig. 6 considering  $OCR = 2.50$ . The mesh deformation referred to the nonlinear analysis is clearly smaller than that obtained with the linear model, although both results show expressive lateral displacements at nodes beneath the footing location. Differences are evidenced in the comparisons performed in terms of stress distributions, especially for the shear component  $\sigma_{xz}$ .

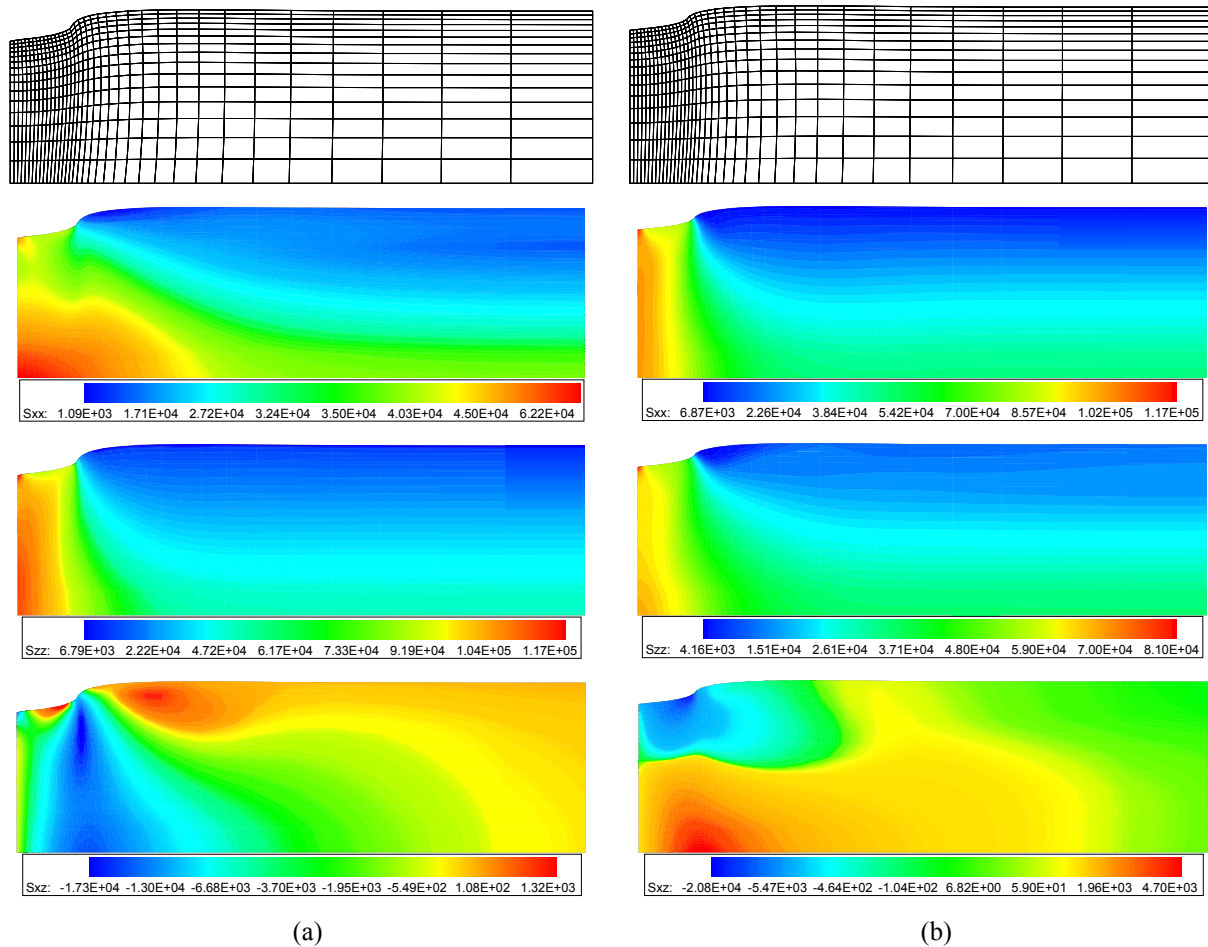


Figure 6. Final stress components and final mesh configurations: (a) geometrically linear analysis; (b) geometrically nonlinear analysis.

### 4.3. Three-dimensional analyses of a flexible footing

The numerical model proposed in this work is verified in this section using a numerical test that demonstrates its ability to predict results for three-dimensional stress states. The present application is based on the footing test performed by Lee et al. (2005), where a cubical model under the action of a flexible square footing is investigated.

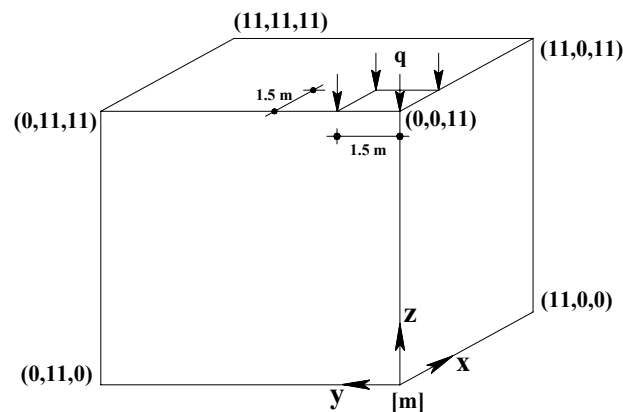


Figure 7. Geometrical and load characteristics considered in the three-dimensional footing analysis.

Geometrical and load characteristics related to the problem studied here are shown in Fig. 7. The computational domain is composed of  $24 \times 24 \times 14$  eight-node hexahedral elements and symmetry boundary conditions are imposed on the planes defined by  $(x,y,z) = (0,0,0)$ . Physical constants adopted in the present simulations are listed in Table 3, which are referred to the Modified Cam-Clay model. Gravity and external loads are applied simultaneously and initial stress

states utilized in the present example are calculated using Eq. (5), which leads to a hydrostatic stress state  $p$  based on the Young's modulus indicated in the reference work and other physical constants presented in Table 3.

Table 3. Physical parameters adopted in the three-dimensional footing analyses.

Young's modulus – E (MPa)	80
Slope of CSL – M	0.898
Slope of NCL – $\lambda$	0.250
Slope of URL – $k$	0.050
Initial void ratio – $e_0$	1.600
Poisson's ratio – $\nu$	0.250
Specific weight – $\gamma$ [KN/m <sup>3</sup> ]	20

A Load-settlement curve obtained in the present simulation is shown in Fig. 8 together with predictions taken from the reference work, where displacements are measured at  $(x,y,z) = (0,0,11)$ . In the elastic range, the response obtained with the present formulation agrees with the numerical predictions observed in Lee et al. (2005). On the other hand, the present plastic response is better correlated with the experimental results indicated in the reference work. These differences may be referred to distinct characteristics observed in the constitutive models compared in this example.

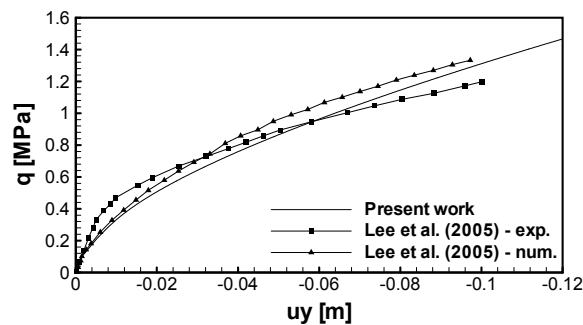


Figure 8. Load-settlement curves obtained in the three-dimensional footing analysis.

Figure 9 illustrates the final mesh configuration obtained in the present simulation. In addition, final stress distributions of  $\sigma_{zz}$  over the computational domain are also shown, where the characteristic compression bulb under the load area is easily identified.

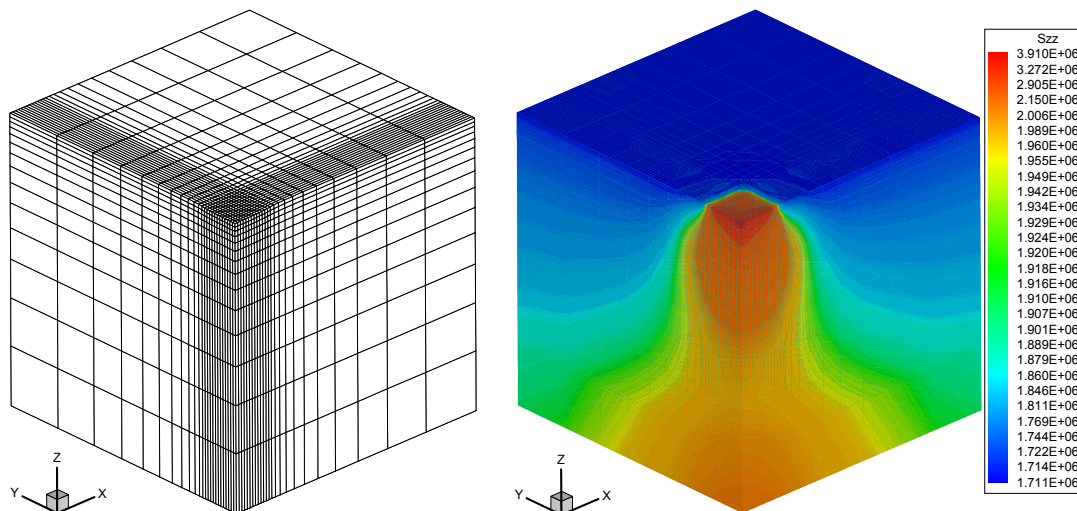


Figure 9. Final mesh configuration and final stress distribution for the three-dimensional footing analysis.

## 5. CONCLUSIONS

A numerical model based on one-point quadrature and critical state formulation was proposed in this work to simulate the mechanical behavior of soils. The critical state formulation was briefly described using a classical

elastoplastic approach where the Modified Cam-Clay model was emphasized. The finite element implementation of the analytical model was performed using the eight-node hexahedral element formulation and reduced integration techniques. A corotational reference system was utilized to stabilize the element formulation as well as to describe stress-strain relations and motion, especially for geometrically nonlinear analysis. The constitutive equation was integrated in this paper using an explicit algorithm with an automatic procedure to split the strain increment into a number of subincrements. Results demonstrated good agreement with the reference works, where experimental predictions were also included. In a future work, the present formulation shall be extended to analyze the mechanical behavior of saturated/unsaturated soils.

## 6. ACKNOWLEDGEMENTS

The authors wish to thank CNPq for the financial support.

## 7. REFERENCES

- Borja, R.I. and Tamagnini, C., 1998, "Cam-clay plasticity. Part III: Extension of the infinitesimal model to include finite strains", *Computer Methods in Applied Mechanics and Engineering*, Vol. 155, pp. 73-95.
- Braun, A.L. and Awruch, A.M., 2008, "Geometrically non-linear analysis in elastodynamics using the eight-node finite element with one-point quadrature and the generalized- $\alpha$  method", *Latin American Journal of Solids and Structures*, Vol. 5, n° 1, pp. 17-45.
- Coulomb, C.A., 1776, "Essai sur une application des règles de maxims et minims à quelques problèmes de statique, relatifs à l'architecture", *Mèm. Acad. R. Sci.*, Vol. 7, pp. 343-382.
- Duarte Filho, L.A. and Awruch, A.M., 2004, "Geometrically nonlinear static and dynamic analysis of shells and plates using the eight-node hexahedral element with one-point quadrature", *Finite Elements in Analysis and Design*, Vol. 40, pp. 1297-1315.
- Flanagan, D.P. and Belytschko, T., 1981, "A uniform strain hexahedron and quadrilateral with orthogonal hourglass control", *International Journal of Numerical Methods in Engineering*, Vol. 17, pp. 679-706.
- Gens, A. and Potts, D.M., 1988, "Critical state models in computational geomechanics", *Engineering Computations*, Vol. 5, pp. 178-197.
- Lee, J., Salgado, R. and Kim, S., 2005, "Bearing capacity of circular footings under surcharge using state-dependent finite element analysis", *Computers and Geotechnics*, Vol. 32, pp. 445-457.
- Potts, D.M. and Ganendra, D., 1994, "An evaluation of substepping and implicit stress point algorithms", *Computer Methods in Applied Mechanics and Engineering*, Vol. 119, pp. 341-354.
- Rankine, W.J.M., 1857, "On the stability of loose earth. *Phil. Trans. R. Soc.*", Vol. 147, pp. 9-27.
- Roscoe, K.H. and Burland, J.B., 1968, "On the generalized stress-strain behaviour of 'wet' clay", In: *Engineering Plasticity*, Cambridge University Press, pp. 535-560.
- Roscoe, K.H. and Schofield, A.N., 1963, "Mechanical behaviour of an idealized 'wet' clay", *Proceedings of the 2<sup>nd</sup> European Conference on Solid Mechanics & Foundation Engineering*, Vol. 1, Wiesbaden, pp. 47-54.
- Schofield, A.N. and Wroth, C.P., 1968, "Critical State Soil Mechanics", McGraw-Hill, London.
- Sheng, D., Sloan, S.W. and Yu, H.S., 2000, "Aspects of finite element implementation of critical state models", *Computational Mechanics*, Vol. 26, pp. 185-196.
- Sloan, S.W., Abbo, A.J. and Sheng, D., 2001, "Refined explicit integration of elastoplastic models with automatic error control", *Engineering Computations*, Vol. 18, n° 1/2, pp. 121-154.
- Xia, K. and Masud, A., 2009, "A stabilized finite element formulation for finite deformation elastoplasticity in geomechanics", *Computers and Geotechnics*, Vol. 36, pp. 396-405.
- Zhao, J., Sheng, D., Rouainia, M. and Sloan, S.W., 2005, "Explicit Integration of complex soil models", *International Journal for Numerical and Analytical Methods in Geomechanics*, Vol. 29, pp. 1209-1229.

## 8. RESPONSIBILITY NOTICE

The authors are the only responsible for the printed material included in this paper.